Stereodynamics study of the $H'(^2S) + NH(X^3\Sigma^-) \rightarrow N(^4S) + H_2$ reaction*

Wei Qiang(魏 强)†

Department of Applied Physics, Chongqing University of Technology, Chongqing 400050, *China*

(Received 6 April 2013; revised manuscript received 8 May 2013; published online 10 December 2013)

The stereodynamics and reaction mechanism of the $H'(^2S) + NH\ (X^3\Sigma^-) \rightarrow N(^4S) + H_2$ reaction are thoroughly studied at collision energies in the 0.1 eV–1.0 eV range using the quasiclassical trajectory (QCT) on the ground $4A''$ potential energy surface (PES). The distributions of vector correlations between products and reagents $P(\theta_r)$, $P(\phi_r)$ and $P(\theta_r, \phi_r)$ are presented and discussed. The results indicate that product rotational angular momentum $\boldsymbol{j}'$ is not only aligned, but also oriented along the direction perpendicular to the scattering plane; further, the product H_2 presents different rotational polarization behaviors for different collision energies. Furthermore, four polarization-dependent differential cross sections (PDDCSs) of the product H_2 are also calculated at different collision energies. The reaction mechanism is analyzed based on the stereodynamics properties. It is found that the abstraction mechanism is appropriate for the title reaction.

Keywords: quasiclassical trajectory, $H' + NH$ reaction, stereodynamics, mechanism

PACS: 34.10.+x, 34.50.–s, 34.50.lf **DOI:** 10.1088/1674-1056/23/2/023401

1. Introduction

The stereodynamics properties from experimental and theoretical investigations provide us with a comprehensive picture of the molecular dynamics and a rigorous description of reactive and nonreactive events.[1] Experimentally, with the development of molecular beam techniques[2] and polarized laser light,[3] precisely controlling and measuring the angular momentum polarization and vector correlations of reagent and product in molecular reactions has nowadays become feasible.[4] From a theoretical point of view, both the quasiclassical trajectories (QCT)[5,6] and the quantum-mechanical (QM)[7] methods have been developed to calculate these stereodynamics properties, such as the rotational alignment parameter and the angular distributions of $P(\theta_r)$, $P(\phi_r)$ and $P(\theta_r, \phi_r)$, as well as the polarization-dependent differential cross sections (PDDCSs). By using QCT and QM methods, the stereodynamic properties of triatomic[8–11] and polyatomic[12,13] reactions have been extensively studied.

The ground state hydrogen reaction $H(^2S) + NH(X^3\Sigma^-)$ plays an important role in the decay of imidogen (NH) in the pyrolysis of ammonia and gas-phase combustion reactions of nitrogen compounds.[14] The earlier experiments have focused on the kinetics features of the title reaction, such as the barrier height, activation energy, and the rate constant.[15–17] Afterward, some *ab initio* calculations and transition state theory (TST), as well as the quasi-classical trajectory (QCT) based on a series of semiempirical and *ab initio* potential energy surfaces (PESs), were performed to justify theses kinetics quantities.[18–24] Up to now, little attention has been paid to the stereodynamics properties of the title reaction. To the best of our knowledge, only Han *et al.*[25] have recently reported on the rotational alignment parameters of the title reaction for the products H_2 by using QCT method based on the DMBE PES constructed by Poveda and Varandas.[24] The result indicates that the angular momentum of the product aligns along the direction perpendicular to the $\boldsymbol{k}$ and the alignment becomes stronger with the increase of collision energy. Very recently, Zhai and Han[26] constructed a new global PES for the ground state ($4A''$) of the title reaction from a set of accurate *ab initio* data by using the many-body expansion and neural network methods. They also calculated the reaction probabilities, integral cross section and rate constants for the title reaction based on their own PES using a three-dimensional (3D) time-dependent wave-packet method. The calculated rate constants are in excellent agreement with the available experimental results. In order to fully understand the title reaction, in this article, we will calculate the three angular distributions of $P(\theta_r)$, $P(\phi_r)$ and $P(\theta_r, \phi_r)$ and four polarization-dependent differential cross sections (PDDCSs) based on this new PES. The reaction mechanism is also discussed based on these stereodynamics properties.

2. Theory

2.1. Quasi-classical trajectory calculations

These calculations were performed by applying a standard QCT-stereodynamics procedure that has been successfully used to study a great many of collision reactions.[27–37] The classical Hamilton equations are numerically integrated in three dimensions. We carry out the calculations of the prod-

*Project supported by the National Natural Science Foundation of China (Grant Nos. 11204392 and 11047125).

†Corresponding author. E-mail: qiangwei@cqut.edu.cn

© 2014 Chinese Physical Society and IOP Publishing Ltd

uct rotational polarization with the initial rotational quantum number $j = 0$ and initial vibrational number $v = 0$. The collision energies are in the range of 0.1 eV–1.0 eV and the initial collision length is 10 Å for each reaction. A batch of 10^5 trajectories is run for each energy and the integration step size in the trajectories is chosen to be 0.1 fs, which guarantees the conservations of the total energy and total angular momentum. The calculations are performed on the newly reported high-quality PES for ground state ($4A''$) constructed by Zhai and Han.[26] The major feature of the PES is that the predicted barrier height is lower than previous theoretical estimates and the heat of reaction with zero-point energy is closer to the experimental values.[26]

2.2. Product rotational polarization

The general theory of the product rotational polarization is standard, so we only provide a simple description relevant to this work. The reference frame used in this work is the center-of-mass (CM) frame, which is shown in Fig. 1. The reagent relative velocity vector $\boldsymbol{k}$ is parallel to the z axis and the $\boldsymbol{x}$–$\boldsymbol{z}$ plane is the scattering plane containing the initial and final relative velocity vectors, $\boldsymbol{k}$ and $\boldsymbol{k}'$. The angle θ_t is the so-called scattering angle between the reagent relative velocity and the product relative velocity. The angles θ_r and ϕ_r are the polar and azimuthal angles of the resultant rotational angular momentum $\boldsymbol{j}'$.

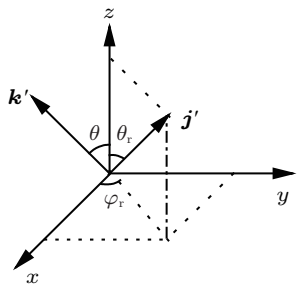


Fig. 1. Center-of-mass coordinate system used to describe the $\boldsymbol{k}$, $\boldsymbol{k}'$ and $\boldsymbol{j}'$ correlations.

The distribution function $P(\theta_r)$ and the dihedral angle distribution function $P(\phi_r)$ describe the $\boldsymbol{k}$–$\boldsymbol{j}'$ and $\boldsymbol{k}$–$\boldsymbol{k}'$–$\boldsymbol{j}'$ correlations, respectively. The function $P(\theta_r)$ can be expanded in a series of Legendre polynomials as[38,39]

$$P(\theta_r) = \frac{1}{2}\sum_k (2k+1)a_0^{(k)} \mathrm{P}_k(\cos\theta_r), \tag{1}$$

where

$$a_0^{(k)} = \int_0^{\pi} P(\theta_r) P_k(\cos\theta_r)\sin\theta_r \mathrm{d}\theta_r = \langle \mathrm{P}_k(\cos\theta_r)\rangle. \tag{2}$$

The expanding coefficients $a_0^{(k)}$ are called the orientation (k is odd) or alignment (k is even) parameters. The dihedral angle distribution function $P(\phi_r)$ can be expanded in a series of Fourier series as

$$P(\phi_r) = \frac{1}{2\pi}\left(1 + \sum_{\text{even},n\geq 2} a_n \cos n\phi_r\right) + \sum_{\text{odd},n\geq 1} b_n(\sin n\phi_r), \tag{3}$$

where

$$a_n = 2\langle \cos n\phi_r\rangle, \tag{4}$$

$$b_n = 2\langle \sin n\phi_r\rangle. \tag{5}$$

In this calculation, $P(\theta_r)$ and $P(\phi_r)$ are expanded up to $k = 18$, $n = 24$, respectively, thereby showing good convergence.

The fully correlated CM angular distribution is written as the sum

$$P(\omega_t, \omega_r) = \sum_{kq} \frac{[k]}{4\pi}\frac{1}{\sigma}\frac{\mathrm{d}\sigma_{kq}}{\mathrm{d}\omega_t} C_{kq}(\theta_t, \theta_r), \tag{6}$$

where $[k] = 2k+1$, $C_{kq}(\theta_t, \theta_r) = \sqrt{4\pi/(2k+1)}\mathrm{Y}_{kq}(\theta_r, \phi_r)$ is modified spherical harmonics, $(1/\sigma)(\mathrm{d}\sigma_{kq}/\mathrm{d}\omega_t)$ is a generalized PDDCSs and yields

$$\frac{1}{\sigma}\frac{\mathrm{d}\sigma_{k0}}{\mathrm{d}\omega_t} = 0, \quad k \text{ is odd}, \tag{7}$$

$$\frac{1}{\sigma}\frac{\mathrm{d}\sigma_{kq+}}{\mathrm{d}\omega_t} = \frac{1}{\sigma}\frac{\mathrm{d}\sigma_{kq}}{\mathrm{d}\omega_t} + \frac{1}{\sigma}\frac{\mathrm{d}\sigma_{k-q}}{\mathrm{d}\omega_t} = 0, \tag{8}$$

k is even and q is odd or k is odd and q is even;

$$\frac{1}{\sigma}\frac{\mathrm{d}\sigma_{kq-}}{\mathrm{d}\omega_t} = \frac{1}{\sigma}\frac{\mathrm{d}\sigma_{kq}}{\mathrm{d}\omega_t} - \frac{1}{\sigma}\frac{\mathrm{d}\sigma_{k-q}}{\mathrm{d}\omega_t} = 0, \tag{9}$$

k is even and q is even or k is odd and q is odd.

The PDDCS can be written as

$$\frac{1}{\sigma}\frac{\mathrm{d}\sigma_{kq\pm}}{\mathrm{d}\omega_t} = \sum_{k1}\frac{k_1}{4\pi} S^{k_1}_{kq\pm} C_{k_1 q}(\theta_t, 0), \tag{10}$$

where $S^{k_1}_{kq\pm}$ is an expected value and written as

$$S^{k_1}_{kq\pm} = \langle C_{k_1 q}(\theta_t, 0) C_{kq}(\theta_r, 0)[(-1^q)\,\mathrm{e}^{\mathrm{i}q\xi\phi_r} \pm \mathrm{e}^{-\mathrm{i}q\phi_r}]\rangle, \tag{11}$$

with the angular brackets denoting the average over all the angles.

In this work, we calculate $(2\pi/\sigma)(\mathrm{d}\sigma_{00}/\mathrm{d}\omega_t)$, $(2\pi/\sigma)(\mathrm{d}\sigma_{20}/\mathrm{d}\omega_t)$, $(2\pi/\sigma)(\mathrm{d}\sigma_{22+}/\mathrm{d}\omega_t)$, and $(2\pi/\sigma)\times(\mathrm{d}\sigma_{21-}/\mathrm{d}\omega_t)$, which are named PDDCS_{00}, PDDCS_{20}, PDDCS_{22+}, and PDDCS_{21-} respectively, in the cases of $k = 0$ and $k = 2$ by using the computational code developed by Chen *et al.* [40]

3. Results and discussion

The distributions of $P(\theta_r)$ for product H_2 at different collision energies are presented in Fig. 2, which describes the $\boldsymbol{k}$–$\boldsymbol{j}'$ correlation. The figure is illustrated on the basis of ten different collision energies ranging from 0.1 eV to 1.0 eV in steps of 0.1 eV. As can be seen from Fig. 2, the $P(\theta_r)$ distributions are symmetric with respect to 90° at all collision

energies, which indicates that the product rotational angular momentum vector is aligned along the direction perpendicular to the relative velocity direction. Moreover, the collision energy has distinct effects on the $P(\theta_r)$ distribution at 0.1 eV–0.5 eV, but not so great at 0.6 eV–1.0 eV. The overall trends of the $P(\theta_r)$ distributions become higher and narrower as the collision energy increases from 0.1 eV–1.0 eV though little fluctuation at 0.6 eV and 0.8 eV. This means that the degree of the rotational alignment of the product becomes stronger with the increase of the collision energy. As is well known, the distribution of $P(\theta_r)$ is correlated to the rotational alignment parameter $\langle P_2(j' \cdot k)\rangle$, which also provides information about the product rotational alignment. Recently, Han *et al.*[25] calculated the $\langle P_2(j' \cdot k)\rangle$ based on DMBE PES in a collision energy range of 2 kcal/mol–20 kcal/mol, which also indicates that the title reaction exhibits stronger product alignment perpendicular to $\boldsymbol{k}$ with collision energy rising.

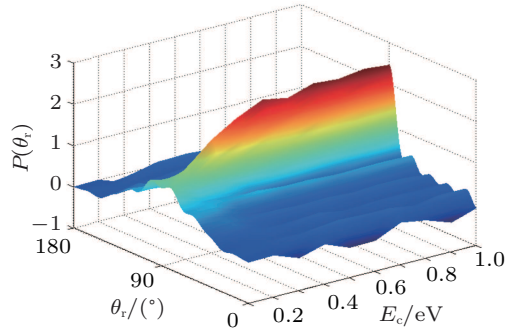


Fig. 2. (color online) Distributions of $P(\theta_r)$ as a function of both the polar angle θ_r and the collision energy in the range 0.1 eV–1.0 eV for the reaction $H' + NH$ ($v = 0$, $j = 0$) $\rightarrow N + H_2$.

The dihedral angle distributions $P(\phi_r)$, shown in Fig. 3, describe the $\boldsymbol{k}$–$\boldsymbol{k}'$–$\boldsymbol{j}'$ correlation, which provides stereodynamical information about both product alignment and orientation. As can be seen from Fig. 3, the distributions $P(\phi_r)$ tend to be strongly asymmetric with respect to the $\boldsymbol{k}$–$\boldsymbol{k}'$ scattering plane (or about $\phi_r = 180^\circ$) because the peaks of $P(\phi_r)$ only appear at $\phi_r = 270^\circ$. Such distributions have also been found in H + HBr[32] reaction, which directly reflect the strong polarization of product angular momentum. The peaks of $P(\phi_r)$ appearing only at $\phi_r = 270^\circ$ indicate that the product rotational angular momentum is not only aligned along the y axis (perpendicular to the scattering plane) but also mainly oriented along the negative direction of the y axis of the CM frame. That is to say, there exists a strong preference for the product molecules to rotate clockwise in the plane parallel to the scattering plane. Thus, we can roughly obtain the picture of this reaction that the reaction happens much easier to when the reactant relative velocity $\boldsymbol{k}$ is parallel to the plane containing the three reactive atoms, or that the PES tends to rotate the three atoms into a plane parallel to $\boldsymbol{k}$ to proceed with the reaction. It is should be mentioned that the peaks of $P(\phi_r)$ show a decrease somewhat, as the collision energy increases from 0.7 eV to 1.0 eV. The reason is maybe due to the features of the PES used in this work. The potential barrier is 28.8 kcal/mol for collinear geometry and increases with the H′–H–N angle decreasing. So, the reaction can occur through more configurations at higher energies than at lower energies and then the different structures of transition states cause the values of $P(\phi_r)$ to decrease little.

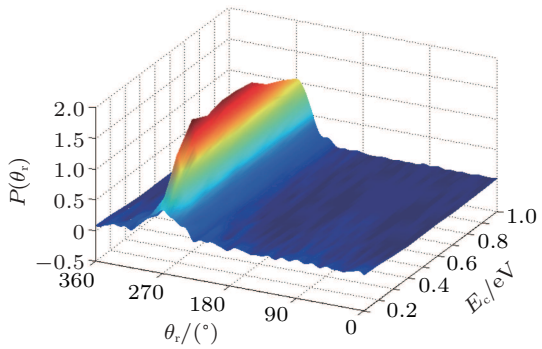


Fig. 3. (color online) The $P(\phi_r)$ distributions as a function of both the dihedral angle ϕ_r and collision energy in the range 0.1 eV–1.0 eV for the reaction $H' + NH$ ($v = 0$, $j = 0$) $\rightarrow N + H_2$.

According to the impulsive model of the atom and molecule reaction A + BC→AB + C,[38] $\boldsymbol{j}' = \boldsymbol{L}\sin^2\beta + \boldsymbol{j}\cos^2\beta + \boldsymbol{J}_1 m_B/m_{AB}$, where $\boldsymbol{L}$ is the reagent orbital angular momentum, $\boldsymbol{J}_1 = \sqrt{\mu_{BC}R}(r_{AB} \times r_{BC})$, with r_{AB} and r_{BC} being the unit vectors and B pointing to A and C, respectively, μ_{BC} is the reduced mass of the BC molecule and R is the repulsive energy between B and C atoms. During the chemical reaction, $\boldsymbol{L}\sin^2\beta + \boldsymbol{j}\cos^2\beta$ is symmetric with respect to the $\boldsymbol{k}$–$\boldsymbol{k}'$ scattering plane, whereas $\boldsymbol{J}_1 m_B/m_{AB}$ tends to a preferential direction due to the repulsive energy, which leads to the orientation of $\boldsymbol{j}'$. Obviously, the repulsive energy is closely related to the properties of PES. Here, we recall the PES used in this work, as the H′ comes to NH with the N–H–H′ angles being 180°, 120°, 90°, and 30°, there is a late barrier in the collinear geometry and the barrier increases as the N–H–H′ angle decreases.[26] It is clear that the PES used in this work is a typical repulsive PES, which acts as an important role for alignment and orientation of the product. The late high barrier leads to strong rotational alignment/orientation, which was also found in H/D + FO[31] and H + HBr reactions.[32]

Furthermore, as discussed in Refs. [42] and [43], the different orientations of $\boldsymbol{j}'$ are associated with different reaction mechanisms, such as abstraction and insertion mechanisms. As to the title reaction, if the reaction is dominated by the abstraction mechanism, forming the metastable and short lived intermediate H′–H–N (the incoming H′ atom attacks the H atom of the H–N), the product rotational angular momentum $\boldsymbol{j}'$ will be oriented along a specific direction (for example, the negative direction of the y axis); if the reaction is dominated

by the insertion mechanism, forming the stable and long-lived complex H–H′–N (the incoming H′ atom inserted between the H atom and the N atom), the product rotational angular momentum $\boldsymbol{j}'$ will be oriented along another specific direction (for example, the positive direction of the y axis). As to the title reaction, only the peak of $P(\phi_r)$ at 90° is found, which directly suggests the title reaction may be controlled by a reaction mechanism. In order to confirm which one is suitable for the title reaction, we also calculate the internulcear distance between the three atoms for the title reaction at 0.1, 0.6 and 1 eV, which provides a vivid way to understand the reaction mechanism. As can be seen from Fig. 4, most reactive trajectories undergo a short collision time ($\leq$ 200 fs), which clearly shows that the lifetime of the complex is very short and the reaction is dominated by the abstraction mechanism. That is to say, the incoming H′ atom attacks the H of the H–N and then dissociated into H H′ + N by forming short-lived complex H′–H–N.

We also plot the angular momentum polarization in the form of a polar plot of θ_r and ϕ_r averaged over all scattering angles in Fig. 5. The distributions of $P(\theta_r, \phi_r)$ are in good consistence with the separate $P(\theta_r)$ and $P(\phi_r)$ distributions, which also indicates that the products are strongly polarized in the direction perpendicular to the scattering plane and the products of reaction mainly rotate in planes parallel to the scattering plane. As shown in Fig. 5(e), for the $P(\theta_r, \phi_r)$ distribution at 0.5 eV, the peak is almost at (90°, 270°), directly reflecting the characteristics of the $P(\theta_r)$ and $P(\phi_r)$ distributions at this investigated collision energy. The same things can be found for the other investigated collision energies.

Four PDDCSs of the product H_2 for the title reaction calculated at ten different collision energies are presented in Fig. 6. As is well known, the $PDDCS_{00}$ is independent of product polarization parameters θ_r and ϕ_r, reflecting only the scattered behaviors of the products, which is a simple differential cross section. As can be seen from Fig. 6(a), the distribution of $PDDCS_{00}$ is clearly dominated by a strong backwards peak and a much smaller forwards scattering. The intensities of sideways and backwards scatter decrease with the increase of collision energy. The $PDDCS_{20}$ is the expectation value of the second Legendre moment $\langle P_2 \cos(\theta_r) \rangle$. In Fig. 6(b), $PDDCS_{20}$ is negative for the backwards and sideways scattered products and approximately zero for the forwards scattered products. The tendency of the $PDDCS_{20}$ is basically opposite to the $PDDCS_{00}$, which indicates that $\boldsymbol{j}'$ is preferentially polarized along the direction perpendicular to $\boldsymbol{k}$. Clearly, as the energy increases from 0.1 eV to 1 eV, the degrees of the rotational alignments of the products decrease for backwards scattered product. The $PDDCS_{22+}$ is a reflection of the tendency alignment direction with a value of $\langle \sin^2 \theta_r \cos 2\phi_r \rangle$; the

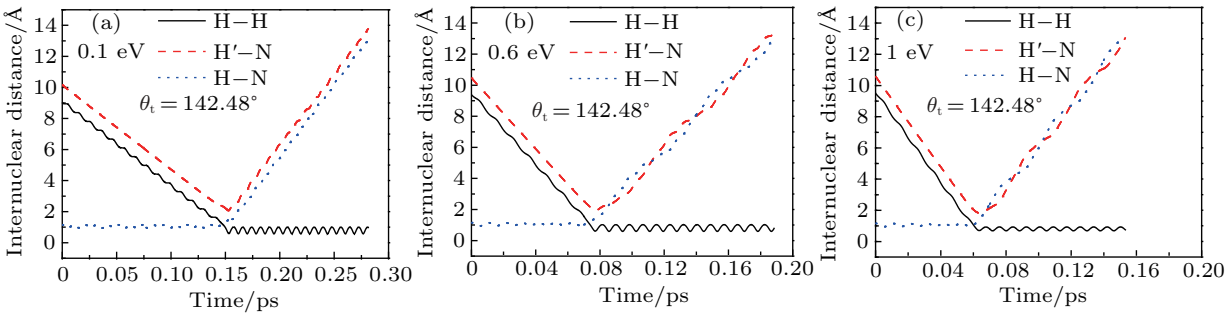


Fig. 4. (color online) Internuclear distances of H′–H, H′–N and H–N as a function of propagating time at collision energy E_{col} = 0.1, 0.6 and 1 eV, with scattering angle θ = 142.480°.

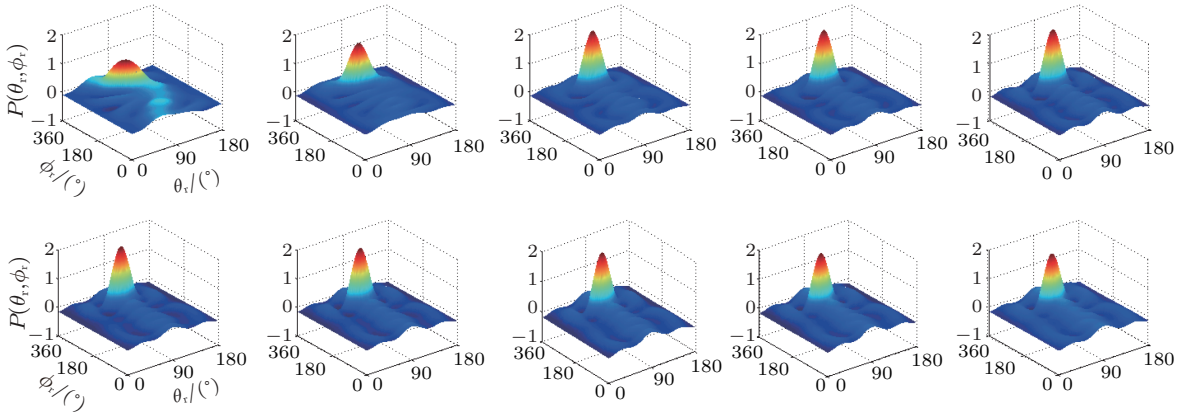


Fig. 5. (color online) Ten joint $P(\theta_r, \phi_r)$ distributions as a function of both polar angles θ_r and ϕ_r for the reaction H′ + NH ($v = 0, j = 0$) → N + H_2 at the collision energies of 0.1 eV–1.0 eV.

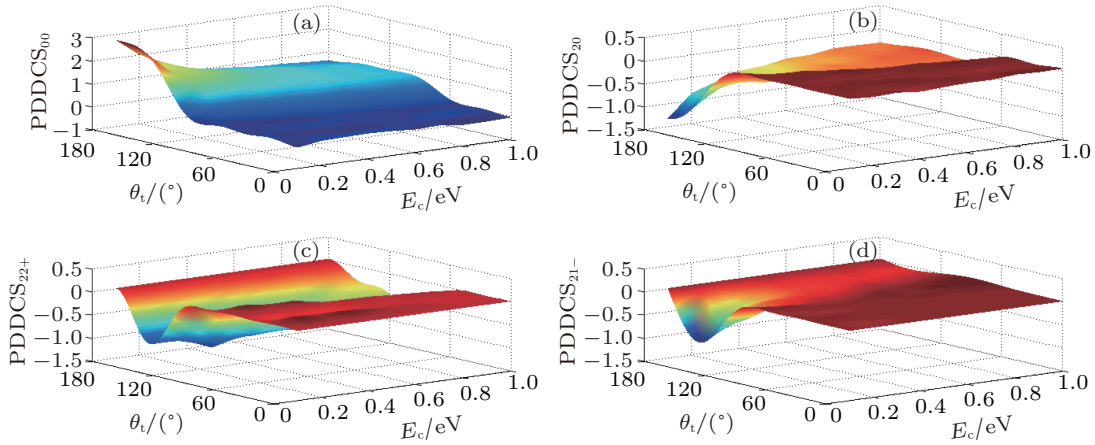


Fig. 6. (color online) Four PDDCSs (PDDCS$_{00}$, PDDCS$_{20}$, PDDCS$_{22+}$, PDDCS$_{21-}$) each as a function of both the scattering angle θ_t and collision energy in the range 0.1 eV–1.0 eV for the reaction H′ + NH ($v = 0, j = 0$) → N + H$_2$.

positive value PDDCS$_{22+}$ reveals the product alignment along the x axis. Conversely, the alignment is along the y axis. The larger absolute value suggests the stronger alignment along the relevant axis. Moreover, if the value is close to zero, there are no obvious alignment directions. From Fig. 6(c), one can find that the values of PDDCS$_{22+}$ are zero for scattering angles below 80°, which clearly suggests that the rotational momentum distributions are all isotropic for these scattering angles. As the angle is larger than 80°, the value is almost negative and with a peak at about 140°, which means the rotational momentum is anisotropic and with the alignment preferentially along the y axis, especially at 140°, the rotational momentum has the strongest alignment along the y axis. The value of PDDCS$_{21-}$ is similar to that of PDDCS$_{22+}$, i.e. $\langle -\sin 2\theta_r \cos\phi_r \rangle$ and is shown in Fig. 6(d). One could clearly distinguish whether the product is aligned along the direction of the vector $\boldsymbol{x}$–$\boldsymbol{z}$ or $\boldsymbol{x}+\boldsymbol{z}$. The positive value PDDCS$_{21-}$ reveals the product alignment along the $\boldsymbol{x}$–$\boldsymbol{z}$ axis. Conversely, the alignment is along the $\boldsymbol{x}+\boldsymbol{z}$ axis and the value is close to zero, implying there are no obvious alignment directions. Generally, the larger absolute value suggests the stronger alignment along the relevant axis. As can be seen from Fig. 6(d), at collision energies of 0.1 eV–0.4 eV, the values of PDDCS$_{21-}$ are almost zero as the scattering angle is smaller than 100° and negative as the scattering angle is larger than 100°, with a peak being at about 155°. This reveals that the rotational angular momentum distributions are almost isotropic at the scattering angles smaller than 100° and align along the $\boldsymbol{x}+\boldsymbol{z}$ axis in scattering angles of 100°–180°. In addition, with collision energy increasing from 0.5 eV to 1.0 eV, the values of PDDCS$_{21-}$ are almost zero for all scattering angles, which suggests the rotational momentum distributions are almost isotropic.

4. Conclusions

In this paper, the stereodynamic properties $P(\theta_r)$, $P(\phi_r)$, $P(\theta_r, \phi_r)$ as well as four normalized PDDCSs are calculated at different collision energies by means of the QCT method. The results indicate that rotational angular momentum vector $\boldsymbol{j}'$ of product H$_2$ is preferentially aligned along the direction perpendicular to $\boldsymbol{k}$ and is also oriented with respect to the $\boldsymbol{k}$–$\boldsymbol{k}'$ plane at all collision energies. The intensity of $P(\theta_r)$ increases with energy increasing, but the intensity of $P(\phi_r)$ has an opposite trend. The PDDCS$_{00}$ shows that the product H$_2$ experiences preferentially backward scattering and begins to decrease when the collision energy increases. Other PDDCSs indicate that the effects of product rotational alignment become weaker with the increase of the collision energy. According to the calculated stereodynamics results, the relevant mechanism is proposed for the title reaction and the reaction proceeds via the short-lived metastable intermediate H′–H–N.

Acknowledgment

The author thanks professor Han Ke-Li for providing the QCT code of stereodynamics and Yue Xian-Fang and Duan Zhi-Xing for helpful discussion.

References

[1] Bernstein R B, Herschbach D R and Levine R D 1987 *J. Phys. Chem.* **91** 5365
[2] Mcclelland G M and Herschbach D R 1979 *J. Phys. Chem. A* **83** 1445
[3] Jonah C D, Zare R N and Ottinger C 1972 *J. Chem. Phys.* **56** 263
[4] Vallance C 2011 *Phys. Chem. Chem. Phys.* **13** 14427
[5] Han K L, He G Z and Lou N Q 1993 *Chin. Phys. Lett.* **10** 517
[6] Han K L, He G Z and Lou N Q 1996 *J. Chem. Phys.* **105** 8699
[7] De Miranda M P and Clary D C 1997 *J. Chem. Phys.* **106** 4509
[8] Xu Y, Zhao J, Yue D G, Liu H, Zheng X Y and Meng Q T 2009 *Chin. Phys. B* **18** 5308
[9] Li X H, Wang M S, Pino H, Yang C L and Ma L Z 2009 *Phys. Chem. Chem. Phys.* **11** 10438
[10] Duan L H, Zhang W Q, Xu X S, Cong S L and Chen M D 2009 *Mol. Phys.* **107** 2579
[11] Xu W W, Liu X G, Luan S X, Sun S S and Zhang Q G 2009 *Chin. Phys. B* **18** 339
[12] Garcia J E 2007 *J. Phys. Chem. A* **111** 5792
[13] Czakó G and Bowman J M 2009 *J. Chem. Phys.* **131** 244302
[14] Miller J A and Bowman C T 1989 *Energy Combust. Sci.* **15** 287
[15] Koshi M, Yoshimura M, Fukuda K, Matsui H, Saito K, Watanabe M, Imamura A and Chen C X 1990 *J. Chem. Phys.* **93** 8703

[16] Davidson D F and Hanson R K 1990 *Int. J. Chem. Kin.* **22** 843
[17] Adam L, Hack W, Zhu H, Qu Z W and Schinke R 2005 *J. Chem. Phys.* **122** 114301
[18] Xu Z F, Fang D C and Fu X Y 1997 *J. Phys. Chem. A* **101** 4432
[19] Zhai H S and Zhou P W 2012 *Chin. Phys. Lett.* **29** 063401
[20] Werner H J and Knowles P J 1988 *J. Chem. Phys.* **89** 5803
[21] Pascual R, Schatz G C, Lendvay G and Troya D 2002 *J. Phys. Chem. A* **106** 4125
[22] Jordan M J T, Thompson K C and Collins M A 1995 *J. Chem. Phys.* **102** 5647
[23] Poveda L A and Varandas A J C 2006 *Theor. Chem. Acc.* **116** 404
[24] Poveda L A and Varandas A J C 2005 *Phys. Chem. Chem. Phys.* **7** 2867
[25] Han B R, Yang H, Zheng Y J and Varandas A J C 2010 *Chem. Phys. Lett.* **493** 225
[26] Zhai H S and Han K L 2011 *J. Chem. Phys.* **135** 104314
[27] Duan Z X, Li W L and Qiu M H 2012 *J. Chem. Phys.* **136** 144309
[28] Yue X F 2012 *Chin. Phys. B* **21** 073401
[29] Liu Y F, He X H, Shi D H and Sun J F 2011 *Chin. Phys. B* **20** 078201
[30] Li X H, Wang M S, Pino H, Yang C L and Ma L Z 2009 *Phys. Chem. Chem. Phys.* **11** 10438
[31] Chu T S 2009 *J. Comput. Chem.* **31** 1385
[32] Zhang W Q, Cong S L, Zhang C H, Xu X S and Chen M D 2009 *J. Phys. Chem. A* **113** 4192
[33] Ge M H and Zheng Y J 2011 *Chin. Phys. B* **20** 083401
[34] Yang T G, Yuan J C, Cheng D H and Chen M D 2013 *Commn. Comput. Chem.* **1** 15
[35] Bai M M, Ge M H, Yang H and Zheng Y J 2012 *Chin. Phys. B* **21** 123401
[36] Zhang W Q, Li Y Z, Xu X S and Chen M D 2010 *Chem. Phys.* **367** 115
[37] Xiao J, Yang C L and Wang M S 2012 *Chin. Phys. B* **21** 043101
[38] Li R J, Han K L, Li F E, He G Z and Lou N Q 1994 *Chem. Phys. Lett.* **220** 281
[39] Chen M D, Han K L and Lou N Q 2002 *Chem. Phys. Lett.* **357** 483
[40] Chen M D, Han K L and Lou N Q 2003 *J. Chem. Phys.* **118** 4463
[41] Han K L, He G Z and Lou N Q 1989 *Chin. J. Chem. Phys.* **2** 323
[42] Ding Y J and Shi Y 2011 *Comput. Theor. Chem.* **963** 306
[43] Liu S L and Shi Y 2011 *Chin. Phys. B* **20** 013404